

Dynamical formation of X-ray binaries in the inner bulge of M31

R. Voss^{1*} and M. Gilfanov^{1,2*}

¹Max Planck Institut für Astrophysik, Karl-Schwarzschild-Str.1, 85741 Garching, Germany

²Space Research Institute, Russian Academy of Sciences, Profsoyuznaya 84/32, 117997 Moscow, Russia

ABSTRACT

The radial distribution of luminous ($L_X > 10^{36}$ erg s⁻¹) X-ray point sources in the bulge of M31 is investigated using archival *Chandra* observations. We find a significant increase of the specific frequency of X-ray sources, per unit stellar mass, within 1 arcmin from the centre of the galaxy. The radial distribution of surplus sources in this region follows the ρ_*^2 law, suggesting that they are low-mass X-ray binaries formed dynamically in the dense inner bulge. We investigate dynamical formation of LMXBs, paying particular attention to the high velocity regime characteristic for galactic bulges, which has not been explored previously. Our calculations suggest that the majority of the surplus sources are formed in tidal captures of black holes by main sequence stars of low mass, $M_* \sim 0.4M_\odot$, with some contribution of NS systems of same type. Due to the small size of the accretion discs a fraction of such systems may be persistent X-ray sources. Some of sources may be ultra-compact X-ray binaries with helium star/white dwarf companions. We also predict a large number of faint transients, both NS and BH systems, within ~ 1 arcmin from the M31 galactic centre. Finally, we consider the population of dynamically formed binaries in Galactic globular clusters, emphasizing the differences between these two types of stellar environments.

Key words: galaxies: individual: M31 – X-rays: binaries – X-rays: galaxies

1 INTRODUCTION

It is a well known fact that the ratio of the number of low mass X-ray binaries (LMXBs) to stellar mass is \sim two orders of magnitude higher in globular clusters (GCs) than in the Galactic disc (Clark 1975). With the advent of *Chandra* and *XMM-Newton*, studies of X-ray point sources in external galaxies have become possible, and have shown that also there globular clusters are especially abundant in LMXBs. This is attributed to dynamical processes, through which LMXBs are formed in two-body encounters. Due to the ρ_*^2 dependence on the stellar density such encounters are frequent in globular clusters and are negligible in the field. Currently, there are 13 LMXBs (Liu et al. 2001) in the 150 globular clusters (Harris 1996) known in the Galaxy.

In the central parts of massive galaxies, the stellar densities can reach values similar to the densities in less luminous GCs. Except for the very inner parts, these densities are still an order of magnitude smaller than the densities found in the most luminous GCs, where the LMXBs are preferentially found. However, the large volume compensates for the smaller density and LMXBs can be formed near the galactic centres in two-body encounters in non-negligible numbers. Whereas dynamical interactions in globular clusters have been intensively investigated, the parameter range typical of galactic centres remains unexplored. Due to an order of

magnitude higher stellar velocities, the character of the dynamical interactions and relative importance of different formation channels in the galactic centres differ from those in globular clusters.

Due to the large stellar mass contained in the central region of a galaxy, a number of “primordial” LMXBs formed through the standard evolutionary path exist there too. Although these can not be easily distinguished from the binaries formed in two-body encounters, an argument of the specific LMXB frequency (per unit stellar mass) can be employed, in the manner similar to the one that led to the discovery of dynamical formation of binaries in globular clusters. The volume density of the primordial LMXBs follows the distribution of the stellar mass in a galaxy (Gilfanov 2004) whereas the spatial distribution of the dynamically formed binaries is expected to obey the ρ_*^2/v law (Fabian et al. 1975). Hence the latter should be expected to be much more concentrated towards the centre of the host galaxy and reveal themselves as a population of “surplus” sources near its centre.

M31 is the closest galaxy with a bulge density large enough to host a number of LMXBs formed through dynamical interactions. At a distance of 780 kpc (Stanek & Garnavich 1998; Macri et al. 2001) X-ray sources can be easily resolved with *Chandra*, even near the centre of the galaxy. It has been studied extensively with *Chandra* and we use these observations to explore the radial distribution of bright X-ray point sources in the bulge. The results of this study are presented in the Section 2 where it is demonstrated that the specific frequency of X-rays sources increases sharply inside ≈ 1 arcmin. The possible nature of surplus sources is discussed in

* E-mail: voss@mpa-garching.mpg.de (RV); gilfanov@mpa-garching.mpg.de (MG)

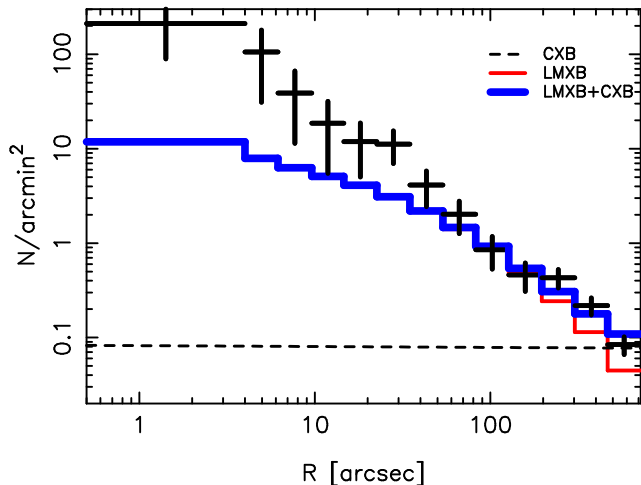


Figure 1. The radial distribution of the X-ray point sources in M31, excluding globular cluster sources. The histograms show the total distribution and individual components of the model: flat distribution of CXB sources and primordial LMXB sub-population tracing the stellar mass distribution. The normalizations of the individual components are from the best fit to the data outside 1 arcmin.

section 3. The details of dynamical formation of binaries in dense stellar environments and dependence on the stellar velocity dispersion are considered in the section 4. The results of this section are applied to the inner bulge of M31 and to the Galactic globular clusters in sections 5. Our conclusions are presented in the section 6.

2 RADIAL DISTRIBUTION OF THE X-RAY POINT SOURCES

With the currently available *Chandra* data it is possible to study the spatial distribution of the X-ray point sources in the bulge, without being affected by incompleteness, down to the limiting luminosity of 10^{36} erg s^{-1} . We restrict our analysis out to a distance of 12 arcmin from the centre and combine 26 ACIS observations with telescope pointings within the central 10 arcmin region of the M31 bulge for a total exposure time of 201 ks. Details of the data analysis, the source lists and the luminosity functions of various sub-populations in the bulge are presented in Voss & Gilfanov (2007).

We model the radial distribution of the X-ray sources by a superposition of primordial LMXBs and CXB sources, as in Voss & Gilfanov (2006). The spatial distribution of the former is assumed to follow the stellar mass distribution of the galaxy, as traced by the K-band light (Gilfanov 2004). We used the K-band image of M31 provided by 2MASS LGA (Jarret et al. 2003). The distribution of CXB sources is assumed to be flat on the angular scales of interest. Before proceeding with the fit we removed the contribution from sources other than primordial LMXBs and background galaxies. Firstly, we removed 4 identified foreground sources, 1 supernova remnant and one extended source. Secondly, we excluded X-ray binaries associated with globular clusters, as their origin and spatial distribution are different from the “field” LMXBs.

Among our X-ray sources 13 are coincident with confirmed GCs from Galleti et al. (2004) and 8 with GC candidates. We estimated the number of random matches by displacing the sources by 10 arcsec in 4 directions. We found an average of 0.25 coincidences with confirmed GCs and 1.0 with GC candidates. It is well known

that the inner parts of M31 are depleted of GCs, suggesting that the GC list might be affected by incompleteness. Barnby & Huchra (2001) estimate that 70 per cent of the GCs in the central parts of M31 have been detected, leaving the room for only a relatively small number of undetected GCs. As only a small fraction, $\sim 1/5$, of the GCs contain LMXBs it is reasonable to neglect the possible contribution of missing GCs. A large fraction of the GC candidates are not real globular clusters. However, an association with an X-ray source raises the probability of the GC candidates actually being GCs considerably. We therefore remove these sources from our source list too, noting that all conclusions of this paper remain unchanged if the analysis is performed with a source list in which these sources are included.

We fit the relative normalizations of the LMXBs and CXBs, using the maximum likelihood (ML) test. The best fit is given by a model, in which the normalization of CXBs is zero, meaning that all the sources are LMXBs. As an alternative, we performed a χ^2 -fit on the binned data, with > 15 sources in each bin, and obtained the same result. The probability that the data can be a realization of the model is 0.06 using the Kolmogorov-Smirnov (KS) test, and $6 \cdot 10^{-4}$ for the χ^2 test. The KS test is less sensitive to deviations at the end of a distribution, and therefore the result of the χ^2 -test is more restrictive. We conclude that the LMXB+CXB model is rejected.

The visual examination of the data (Fig. 1) suggests that the reason for the rejection of the model is an overdensity of sources in the inner 1 arcmin region of M31. Motivated by this we did a χ^2 fit of the same model to the distribution outside 1 arcmin. The best fit value of the normalization of the CXB component gives the total number of 26 ± 9 sources CXB sources in the entire $r < 12$ arcmin. This value is consistent with the expectation of 29 background galaxies, estimated from the soft band of Moretti et al. (2003), using the method described in Voss & Gilfanov (2006). We therefore fix the normalization of the CXB component at the value corresponding to 29 sources. This gives a total number of the LMXBs of 64 ± 7 in the entire $r < 12$ arcmin image. The χ^2 -value is 2.63 for 3 degrees of freedom. The best fit model is shown in Fig. 1 together with the observed distribution.

Using the best-fit model it is possible to investigate the distribution of sources in the inner 1 arcmin and quantify the excess in the surface density of the sources. The total number of sources detected in the the $r < 60$ arcsec region is 29. The extrapolation of the best fit model into this region predicts 8.4 ± 0.9 sources, and therefore the number of surplus sources is 20.6 ± 5.5 . The error in the latter estimate accounts for the Poissonian uncertainty in the total number of sources inside 60 arcsec and for the uncertainty of the best fit model normalization. As it is obvious from Fig.1, the contrast between the observed number of sources and that predicted from the K-band light distribution increases towards the centre of the galaxy. Inside $r < 15$ arcsec, for example, 9 sources are detected with only 1.1 sources predicted. The formal probability of such an excess to happen due to statistical fluctuation is $\sim 3 \cdot 10^{-6}$, assuming Poissonian distribution.

3 ORIGIN OF THE SURPLUS BINARIES

Non-uniform extinction, peaking at the centre of M31, could cause the distribution of the K-band light to deviate from the distribution of stellar mass. This possibility can be excluded, however, as the extinction towards the centre of M31 is low, $A_V=0.24$ mag and $A_I=0.14$ mag (Han 1996), which extrapolated to the K-band gives

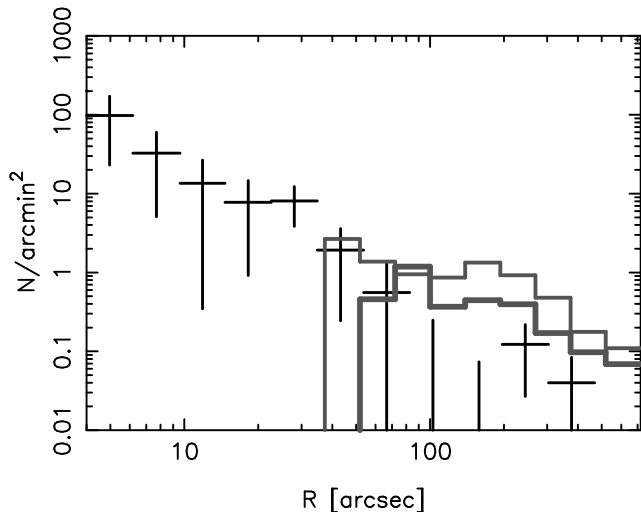


Figure 2. The radial distribution of the “surplus” X-ray sources, computed as a difference between the data and best fit model shown in figure 1. The histograms show distributions of the confirmed globular clusters (thick grey line) and globular cluster candidates (thin grey line).

$A_K=0.03$ (Binney & Merrifield 1998). Moreover, a non-uniform extinction distribution would also cause non-uniformity in the apparent colours of the stellar population, which is not observed (Walterbos & Kennicutt 1987).

The surplus sources can be high-mass X-ray binaries associated with star formation in the inner bulge of M31. We derive upper limits for the star formation rate and the number of HMXBs from the $H\alpha$ and FIR luminosities reported by Devereux et al. (1994). The combined $H\alpha$ luminosity of the nuclear region and from diffuse emission inside the star forming ring (which lies at a radius ~ 50 arcmin, i.e. much larger than the region analysed in this paper) is $4.3 \cdot 10^{39}$ erg s^{-1} (transformed to the distance of 780 kpc used in this paper). From Grimm et al. (2003) we find that this corresponds to 3.2 HMXBs with a luminosity above 10^{36} erg s^{-1} . The FIR luminosity in this region is $5.25 \cdot 10^8 L_\odot$, which corresponds to 5.9 HMXBs with a luminosity above 10^{36} erg s^{-1} .

It should be stressed out, that the region these luminosities refer to is almost 20 times larger than the region analysed in this paper. Moreover it is very likely that the main part of the $H\alpha$ and FIR emission is not associated with star formation, as the number of O-type stars is a factor of ~ 200 lower than what would be expected otherwise (Devereux et al. 1994). To conclude, the HMXB nature of the sources in the inner bulge can be excluded.

The surplus sources could have been created in globular clusters that remain undetected. In the catalogue of Galleti et al. (2004) there are 64 confirmed GCs hosting 13 LMXBs in the region we analysed. The fraction of GCs containing X-ray sources is therefore 0.2. This number is larger than what is found in other galaxies (Sarazin et al. 2003; Maccarone et al. 2003), but consistent with the results for the inner parts of galaxies in Kim et al. (2006). Attributing the ≈ 20 surplus sources to undetected GCs would therefore indicate that ~ 100 unobserved GCs exist in the inner 1 arcmin region of M31. This is much larger than allowed by the completeness level of the present studies of GC population in M31, consistent with only a few undetected globular clusters in this region (Barmby & Huchra 2001).

In a related scenario, the surplus sources could have been created in globular clusters at larger distances from the centre of M31. Due to the mass segregation the globular clusters drift towards the

centre of the bulge, where they are destroyed, leaving behind remnant LMXBs. This scenario has been motivated by Fig.2 where the radial distribution of surplus sources is compared with that of the globular clusters. Indeed, for a GC of mass $10^5 M_\odot$ the mass segregation timescale is $\sim 10^9$ yr at a radius of 5 arcmin and $\sim 10^{10}$ yr at a radius of 12 arcmin (Spitzer 1969). Assuming that a neutron star turns accreted matter into radiation with an efficiency of ~ 0.2 , the lifetime of an LMXB is $\sim 10^9 m_d / L_{37}$ yr, where m_d is the mass of the donor star at the onset of mass transfer expressed in solar masses, and L_{37} is the average luminosity of an LMXB in units of 10^{37} erg s^{-1} . Taking into account that on average $\sim 1/5$ of GCs in M31 contain LMXBs, a destruction rate of ~ 100 globular clusters per Gyr is required to explain ≈ 20 sources observed near the centre of M31. This number is comparable to the total number of GCs within the entire region analysed in this study, and is ~ 30 per cent of the total number of GCs in M31. As GCs are not continually formed in large numbers in M31, the globular cluster system of this galaxy will not be able to sustain such a destruction rate and, consequently, the population of X-ray sources observed in the inner bulge, for any significant length of time.

Finally, the stellar density in the central part of the M31 bulge, $\sim 10^4 M_\odot/\text{pc}^3$, is high enough that LMXBs can be formed through dynamical interactions in the same manner as in globular clusters. In the following sections we investigate this possibility, and apply it to the population of X-ray sources in the inner bulge of M31 and in globular clusters in the Milky Way.

4 DYNAMICAL INTERACTIONS IN DENSE STELLAR ENVIRONMENTS

We begin with consideration of two-body encounters involving a neutron star. The results of this section are extended to formation of black hole binaries in the section 4.4. There are three main channels of dynamical LMXB formation operating in dense stellar environments:

(i) In a tidal capture of a neutron star (NS) by a non-degenerate single star, a close passage of the two stars induces oscillations in the non-degenerate star, and the energy for this is taken from the orbital energy. If the energy of the oscillations exceeds the originally positive orbital energy, the stars are captured in a bound orbit (Fabian et al. 1975).

(ii) A collision between an NS and an evolved single star on the subgiant or red giant branch (RGB) or the asymptotic giant branch (AGB) can lead to the formation of an X-ray binary, in which the donor star is a white/brown dwarf or a helium star, depending on the evolutionary stage of the evolved star before the collision (Ivanova et al. 2005b). In the case of a white dwarf donor an ultra compact X-ray binary is formed. In this scenario, orbital energy is transferred to the envelope of the evolved star, which is expelled, leaving the NS and the core of the evolved star in a bound orbit (Verbunt 1987).

(iii) In an exchange reaction, an NS exchanges place with a star in a pre-existing binary during a close binary-single encounter (Hills 1976).

In the following we compute cross-sections and rates of these three processes, consider their dependence on the velocity dispersion of the stars and discuss various factor affecting their efficiency in the high velocity regime.

Each of the processes depends on the rate of encounters between two types of objects, which in a unit volume is given by $n_1 n_2 \gamma$, where

$$\gamma = \int_0^\infty F(v_{rel}, \sigma_v) \sigma(v_{rel}, M_1, M_2) v_{rel} dv_{rel} \quad (1)$$

where n_1 and n_2 are the number densities and M_1 and M_2 are the masses of object type 1 and 2, respectively, $\sigma(v_{rel})$ is the cross-section of the encounter, and $F(v_{rel})$ is the distribution of relative velocities at infinity. Assuming that the velocity distributions of the two kinds of objects are both Maxwellian and have the same three-dimensional velocity dispersion σ_v , the distribution of relative velocities is given by

$$F(v_{rel}) dv_{rel} = \left(\frac{4\pi}{3}\right)^{-3/2} \sigma_v^{-3} \exp\left(-\frac{3v_{rel}^2}{4\sigma_v^2}\right) 4\pi v_{rel}^2 dv_{rel} \quad (2)$$

Due to the effect of gravitational focusing, the cross-section for two objects to pass within a distance D of each other is given by

$$\sigma(v_{rel}) = \pi D^2 \left(1 + \frac{2G(M_1 + M_2)}{Dv_{rel}^2}\right) \quad (3)$$

In most cases, the gravitational focusing (the second term in the brackets) dominates. Only for very fast encounters (large D and/or v_{rel}) is $Dv_{rel}^2 > 2G(M_1 + M_2)$. If D is independent on the relative velocity, $\gamma \propto \rho^2/v_{rel}$ for slow encounters, and $\gamma \propto \rho^2 v_{rel}$ for the fast ones.

Several remarks are in place, concerning the subsequent evolution of the newly created binary system with a compact object.

Capture of a neutron star in a bound orbit with a companion will lead to formation of an X-ray binary provided that the companion star will fill its Roche lobe and mass transfer will commence within a reasonable time, shorter than $\sim 5 - 10$ Gyr. If the initial binary separation is too large for this to occur immediately after the capture, it can be decreased in the course of evolution of the binary. There are 3 main mechanisms, which affect the orbital separation: (i) magnetic braking, (ii) gravitational braking and (iii) binary-single interactions. The former two are familiar from the standard theory of the binary evolution (see van den Heuvel 1992, for a review). For the companion mass in the $0.4 - 1.0M_\odot$ range they will bring the system in to the Roche lobe contact within 5 Gyr if the initial orbital separation does not exceed $\sim 3.0 - 7.0R_\odot$ and $\sim 2.5 - 3.0R_\odot$ respectively. The braking mechanism due to interaction of the binary with single ‘‘field’’ stars is specific for high stellar density environments. Its properties are briefly summarized below.

When considering evolution of a binary due to binary-single interactions it is conventional to divide the binaries into soft and hard, depending on the ratio of their binding energy to the kinetic energy of the single star at infinity (Heggie 1975). Soft binaries have relatively wide orbits, and interactions with single stars tend to widen the orbit further or to ionize the binary. Hard binaries, on the contrary, are on average hardened by encounters with single stars (Hut & Bahcall 1983). The effect of this is that over time most binaries with a separation above a critical value are disrupted, while the compact ones become more compact. The boundary between soft and hard binaries depends on the stellar velocity dispersion and the mass ratios and ranges from $a \sim 300 - 1000R_\odot$ in a typical globular cluster to $a \sim \text{few } R_\odot$ in the high velocity environment of the M31 bulge. Due to a linear dependence of the cross-section on the binary separation the collisional braking is mostly important at wide binaries, where magnetic braking and gravitational radiation, decreasing as inverse power of the binary separation, are inefficient.

The initial orbital separation in the binaries produced through tidal captures and collisions with RGB/AGB stars is small and a large fraction of this systems will start mass transfer (i.e. become X-ray sources) soon after their formation. Only a small fraction of them (~ 20 per cent in GCs and ~ 2 per cent in M31) will experience close encounters with single stars significantly affecting their semimajor axis, therefore binary-single interactions are not an important factor in their evolution. Binaries created through exchanges, on the contrary, typically have wider orbits, and the effects of encounters can be important.

If the initial binary separation is large and the braking mechanisms are insufficient to start Roche-lobe overflow, this can occur when the donor star evolves off the main sequence, as a result of its expansion during the giant phase. In these systems the accretion disc is large and X-ray emission from vicinity of the NS is insufficient for the irradiation to keep the entire disc ionized, and they are therefore transient (King et al. 1997). Furthermore, mass transfer can only occur while the donor is on the RGB, which makes the lifetime of such systems short. While they may account for bright sources detected in massive elliptical galaxies (Piro & Bildsten 2002), they are too rare to make a significant contribution to our sample. The NSs in these systems are spun up to become millisecond pulsars, and in the Galactic GCs a large number of these have been observed (Lorimer 2005). After the outer layers of the giant star have been ejected, a binary consisting of a white dwarf and an NS remains. However for the vast majority of the systems the binary separation is too large for mass transfer to begin, and they will therefore not become observable in X-rays.

4.1 Single-single encounters

The formation rates of LMXBs due to tidal captures and stellar collisions can be found by integrating the encounter rate, given by equation 1, over the relevant parts of the mass function of stars $f(M)$. We assume that the latter follows the form of Kroupa (2001), a broken powerlaw with slope 1.3 from $0.1-0.5M_\odot$ and slope 2.3 above $0.5M_\odot$, and is normalized according to

$$\int_{M_{co}}^{M_{max}} f(M) dM = 1.0 \quad (4)$$

where M_{max} is the maximum initial mass of stars that have not yet evolved to become stellar remnants at present, and M_{co} is the lower cut-off mass. The number density of stars is then given by $n_* = \frac{\rho_*}{\langle M \rangle}$, where ρ_* is the stellar mass density. We assume the mass of all neutron stars to be $1.4M_\odot$, and that they are formed from stars with initial mass in the range $8.0 - 30.0M_\odot$. The number density of these can then be expressed as $n_{ns} = f_{ns} \frac{\rho_*}{\langle M \rangle} = f_{ns} n_*$, where $f_{ns} = \int_{8M_\odot}^{30M_\odot} f(M) dM$ (for $M_{co} = 0.1M_\odot$ and $M_{max} = 1.0M_\odot$ $f_{ns} = 0.0068$). We define the rate integrated with the mass function

$$\Gamma = \int \gamma f(M) dM \quad (5)$$

where integration is performed in the relevant initial mass range (see below) and γ is from equation 1. With this definition $n_* n_{ns} \Gamma$ gives the rate of encounters in $\text{s}^{-1} \text{cm}^{-3}$. For the calculation of Γ it is necessary to know the current radius of a star $R(M)$ as a function of its initial mass, as well as its evolutionary stage, which is used to define the mass limits of the integral. These informations we take from stellar isochrones of Girardi et al. (2002).

4.1.1 Collisions

We define an encounter between two stars as a collision if the stars come so close that considerable amounts of material is exchanged between them, and hydrodynamical effects become important. For the collisions with NSs, that are relevant for dynamical formation of LMXBs, we distinguish between collisions with main sequence (MS) or horizontal branch (HB) stars and with evolved stars on the RGB or AGB. Due to the different structure of the stars, the outcome of a collision with a NS is different. Simulations indicate that collisions between an NS and an MS star tend to destroy the MS star (Davies et al. 1992). We expect the same to happen to stars on the HB, as their structure is similar to that of MS stars (Dorman 1992). Collisions of this type are not interesting from the point of view of formation of X-ray binaries. As the envelope of stars on the RGB or AGB is less strongly bound to the core, a collision with an NS can lead to the envelope being expelled. The outcome is a short period binary consisting of the core of the evolved star and the NS. If the evolved star had a degenerate core, an ultra-compact X-ray binary (UCXB) with a white dwarf donor will be formed (Verbunt 1987; Ivanova et al. 2005b; Lombardi et al. 2006). In either case an X-ray binary can be created.

The maximum value of distance at periastron R_{coll} , for which significant amounts of material can be exchanged in an encounter of an NS with a non-degenerate star (with radius R_*) is between R_* and the orbital separation at which the star fills its Roche-lobe (Eggleton 1983):

$$a_{full} = \frac{R_*}{0.49} \left[0.6 + q^{-2/3} \ln(1 + q^{1/3}) \right] \quad (6)$$

where $q = M_*/M_{NS}$. For encounters with NSs, this separation ranges from $\sim 5.4R_*$ to $\sim 2.8R_*$ for stars with masses in the $0.1 - 1.0M_\odot$ range. SPH Simulations of stellar encounters have shown that for $M_* \simeq 1M_\odot$, the value of $R_{coll}/R_* \sim 1.8$ (Davies et al. 1992), which we adopt as the standard value. The value of R_{coll}/R_* given, the encounter rate can be calculated from equations 1-3 and 5 (but see below regarding the choice of integration limits in equation 1).

When considering collisions between NSs and evolved stars, it is important to note that the envelope of a star on the RGB/AGB is loosely bound to the core, and the orbital energy of the two stars at infinity can be comparable to the binding energy of the envelope. It is therefore possible that the envelope is expelled without carrying off enough energy to leave a bound system, or that in the high-velocity encounters, the duration of the interaction is too short for enough energy to be transferred from the NS to the envelope. While simulations indicate that the RG envelope is promptly disrupted, instead of ejected through a common envelope (CE) evolution (Rasio & Shapiro 1991; Lombardi et al. 2006), the energy considerations are similar. Adopting the formalism of Webbink (1984) and de Kool (1990), we assume that the envelope of the RG is ejected, and that energy for this (the binding energy of the envelope E_{bind}) is taken from the orbital energy of the two stars which is therefore changed by ΔE_{orb} . Allowing energy to be lost, e.g. as radiation or as some of the envelope is ejected with a velocity higher than the escape speed, an efficiency parameter α_{ce} is defined, so that $E_{bind} = \alpha_{ce} \Delta E_{orb}$. The binding energy of the RG is given by $E_{bind} = -\frac{1.0}{\lambda} \frac{GM_{env}M}{R}$, where M and R is the mass and radius of the RG, respectively, and M_{env} is the mass of the envelope of the RG. λ is a factor that relates the simplified equation to a precise integral of the gravitational binding energy and internal energy in the envelope of the RG, see e.g. Dewi & Tauris (2000). The change in orbital energy needed to reach an orbit with a separation a_f is given

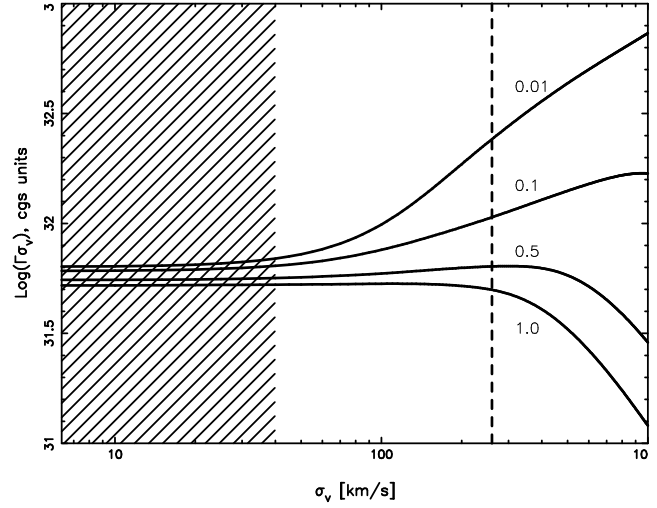


Figure 3. The rate γ of NS-RGB/AGB encounters that lead to the formation of a binary as a function of the 3D velocity dispersion for 4 values of $\alpha_{ce}\lambda$ (equation 7). The values are 0.01, 0.1, 0.5, 1.0 from the top to the bottom. The shaded area corresponds to the range of velocity dispersions in the central parts of GCs, whereas the vertical dashed line corresponds to the velocity dispersion in the bulge of M31.

by $\Delta E_{orb} = \frac{1}{2} \frac{MM_{ns}}{M+M_{ns}} v_{rel}^2 + \frac{GM_{core}M_{ns}}{2a_f}$, where M_{core} is the core mass of the RG, M_{ns} is the mass of the NS and v_{rel} is the relative velocity of the two stars at infinity.

For a given encounter velocity, we can now find the final separation of the binary by solving

$$\frac{GM_{env}M}{R} = \alpha_{ce}\lambda \left(\frac{1}{2} \frac{MM_{ns}}{M+M_{ns}} v_{rel}^2 + \frac{GM_{core}M_{ns}}{2a_f} \right) \quad (7)$$

When we calculate the rate of collisions with evolved stars, γ_{coll} , the integral over velocities (equation 1) is only carried out for velocities $V_{rel} < V_{max,c}$, defined such that the final separation $a_f < 5R_\odot$ (this choice of the maximum separation ensures that the gravitational braking will be efficient on the formed binary)

$$\gamma_{coll} = \int_0^{V_{max,c}} F(v_{rel}, \sigma_v) \sigma_{coll} v_{rel} dv_{rel} \quad (8)$$

where σ_{coll} is the collisional cross-section defined by equation 3 with $D = R_{coll}$. In figure 3 we compare the formation rates of UCXBs due to collisions between RGB+AGB stars and NSs for different values of $\alpha_{ce}\lambda$. The rates were calculated by integrating over all evolutionary stages of stars on the RGB/AGB, using the isochrones of (Girardi et al. 2002). The details of the calculations are given below in section 4.3. It is obvious that the choice of $\alpha_{ce}\lambda$ is very important in the bulge of M31, with an order of magnitude difference between the rates of the highest and the lowest value, while the difference is relatively small in GCs.

SPH simulations indicate that the effectivity in standard CE evolution is $\alpha_{ce} \sim 0.5$ (see Taam & Ricker 2006, and references therein), and in population synthesis studies, values of $\lambda\alpha_{ce}$ in the range 0.1-1.0 are most often assumed (Portegies Zwart & Yungelson 1997; Fryer & Woosley 1999; Hurley et al. 2002; Voss & Tauris 2003; Belczynski et al. 2005), and this seems to give a good fit to the observed properties of the post-CE binary population.

However there are differences between the standard CE evolution and the collisions considered here. In the former, the stars are

already in a bound orbit, and the energy can therefore be transferred to the envelope over a longer period of time during a large number of orbital revolutions. On the other hand, in a collision, enough energy has to be transferred from the NS to the envelope during the first periastron passage, so that the two stars remain bound. Especially for high velocity encounters, the CE formalism might not be directly applicable, as the timescale for the first passage can be so short that the NS passes through the envelope without transferring much energy to this. While the low-velocity regime has been well investigated using SPH simulations (Davies et al. 1992; Lombardi et al. 2006), showing that a value of $R_{coll}/R_* = 1.8$ is adequate, no investigation of the high-velocity regime has been performed. We assume that $\alpha_{ce}\lambda$ is in the range 0.1–1.0 (1.0 can be considered a very conservative estimate, giving the minimum rate of LMXB formation through this process, whereas 0.1 may be a rather optimistic value), with 0.5 being our chosen standard value for calculations below.

4.1.2 Tidal captures

At periastron distances above R_{coll} , and up to a few times R_* , tidal capture can happen. Press & Teukolsky (1977) provided a way of calculating the energy absorbed by the stars assuming $n = 3/2$ polytropes and Lee & Ostriker (1986) extended these calculations to other polytropic indices. In this formulation, the energy of oscillations induced in the non-degenerate star of mass M_* during an encounter with a neutron star is

$$\Delta E_1 = \left(\frac{GM_*}{R_*}\right)^2 \left(\frac{M_{ns}}{M_*}\right)^2 \sum_{l=2,3} \left(\frac{R_*}{R_p}\right)^{2l+2} T_l(\eta) \quad (9)$$

where R_p is the distance of closest approach. Only the spherical harmonic indices $l = 2$ (quadrupole) and $l = 3$ (octupole) are included, as higher indices give negligible contributions to the energy (Lee & Ostriker 1986). The parameter η is defined as

$$\eta = \left(\frac{M_*}{M_* + M_{ns}}\right)^{1/2} \left(\frac{R_p}{R_*}\right)^{3/2} \quad (10)$$

With the tabulated overlap integrals of Lee & Ostriker (1986), for polytropic indices $n = 3/2$ and $n = 3$, we use the numerical method described by Press & Teukolsky (1977) to calculate $T_l(\eta)$. From equation (9) it is then possible to calculate the maximum value of R_p (we call this R_{tid}) for which capture will occur, when the mass of the star and the relative velocity at infinity is known. We use this method for the case where the non-degenerate star is on the MS. A polytropic index of $n = 3/2$ is assumed for the fully convective stars of mass, $M_* < 0.4 M_\odot$, and $n = 3$ for stars $M_* > 0.4 M_\odot$ having radiative core. For stars on the red giant branch, we use the results of McMillan et al. (1990), who calculated R_{tid} for captures of a neutron star by a $0.8 M_\odot$ star at various evolutionary stages along the RGB. This mass is close to the MS turn-off masses for the Galactic globular clusters (GCs), whereas the turn-off mass in M31 is higher, $\sim 1 M_\odot$. We use their results directly in both cases. As tidal captures by evolved stars give a negligible contribution to the overall binary formation rates we did not attempt to perform a more accurate computation for the case of M31. We neglect tidal captures during the subsequent evolutionary stages. The structure of stars on the AGB is similar to those on the RGB, but the time spent there is much shorter. The tidal capture rate must therefore be lower. The time spent on the HB is also very short, compared to the MS lifetime, and although the tidal capture rate may be comparable to the RGB rate, it is much smaller than the MS capture rates.

The tidal capture rate γ_{tidal} is computed as a rate of encounter with the periastron distance $R_{coll} < R_p < R_{tid}$, i.e. contribution of very close encounters resulting in collisions is subtracted:

$$\gamma_{tidal} = \int_0^{v_{max,t}} F(v_{rel}, \sigma_v) [\sigma_{tidal} - \sigma_{coll}] v_{rel} dv_{rel} \quad (11)$$

The upper integration limit $v_{max,t}$ is defined as the velocity at which $R_{coll} = R_{tid}$ i.e. the term in square brackets is required to be positive inside the integration limits. The σ_{tidal} is calculated from equation 3 with $D = R_{tid}$.

Important for the following evolution of tidal capture binaries is the timescale on which the tidally induced oscillations are dissipated. If this timescale is short (as argued by Kumar & Goodman 1996), so that a large fraction of the energy is thermalized within one orbital revolution of the binary, new oscillations will be induced at each periastron passage. The binary quickly becomes circularized with the final orbital separation (from conservation of angular momentum):

$$a = \frac{(\sqrt{2G(M_* + M_{ns})R_p} + v_{rel}R_p)^2}{G(M_* + M_{ns})} \quad (12)$$

For slow encounters (low v_{rel} or small R_p), $a \simeq 2R_p$. If the dissipation time scale is too short, the quick conversion of the energy (of the order of few per cent of the binding energy of the star) may cause the star to expand and lead to a merger. The outcome of the dissipation process depends on the thermalization timescale and the region of the star where the energy is deposited, both factors being unknown (Podsiadlowski 1996). Alternatively, if the dissipation is inefficient, coupling of the orbital motion with oscillation can cause large fluctuations in the orbital energy, substantially extending the circularization process and potentially scattering a fraction of the binaries to wider orbits (Kochanek 1992; Mardling 1995). The details and the final outcome of this processes are poorly understood. In the following we assume that all binaries become circularized with the final separation given by equation 12.

Equation 11 defines the total tidal capture rate, irrespective of the subsequent evolution of the tidally formed binary. In order to calculate the rate of encounters, leading to formation of an LMXB, one needs to account for the finite braking time scales. For this, R_{tid} , used to calculate σ_{tidal} in equation 11, is replaced by $\min(R_{tid}, R_{brake})$, where R_{brake} depends on the mass of the star and is chosen so that the braking time scale for the tidal capture binary is shorter than 5 Gyr. Due to small values of the tidal capture radius R_{tid} , this does not affect the final rates significantly.

4.2 Binary-single interactions

The rate of exchange reactions between a binary (M_1, M_2, a) and a star M_3 is:

$$\gamma_{exch}(M_3, \sigma_v) = \int f(M_1) dM_1 \int p(q) dq \times \int_{a_{min}}^{a_{max}} \gamma(M_1, M_2, M_3, a, \sigma_v) \frac{dn}{da} da \quad (13)$$

where $f(M)$ is the distribution of mass of one of the stars in the binary, q is the binary mass ratio and $p(q)$ its probability distribution, dn/da is the binary semimajor axis distribution and $\gamma(M_1, M_2, M_3, a, \sigma_{rel})$ is the exchange rate of a star M_3 into a binary (M_1, M_2, a) computed from the equation 1. In the context of LMXB formation the third star M_3 is an NS or a black hole.

CO	σ_v (1D)	n_*	f_{ns}	N_{bin}	without collisions				with collisions				
					Total	MS-NS	RG-NS	γ_{ex}	N_{bin}	Total	MS-NS	RG-NS	γ_{ex}
NS	3	$5 \cdot 10^4$	0.0025	1120790	3157	318	816	$1.41 \cdot 10^{32}$	2739700	3093	77	277	$1.39 \cdot 10^{31}$
NS	15	$3 \cdot 10^5$	0.0025	467000	1256	163	277	$2.89 \cdot 10^{31}$	1027400	1328	27	108	$2.17 \cdot 10^{30}$
NS	150	10^4	0.0068	$1.68 \cdot 10^{8\dagger}$	1625	66	165	$1.02 \cdot 10^{29\dagger}$	$8.87 \cdot 10^{7\dagger}$	604	3	46	$8.76 \cdot 10^{27\dagger}$
BH	150	10^4	0.0012	$8.10 \cdot 10^{7\dagger}$	10938	82	739	$1.49 \cdot 10^{30 \dagger}$	$8.10 \cdot 10^{7\dagger}$	9557	13	559	$2.37 \cdot 10^{29\dagger}$

\dagger This simulation was performed for a limited range of orbital separations and γ_{ex} have been corrected for this.

Table 1. Parameters and results for the three simulations of exchange reactions. The parameters are: the velocity dispersion σ_v in km s^{-1} , the number density of single stars n_* in pc^{-3} , the NS fraction in the population of single stars f_{ns} and the number of binaries simulated N_{bin} . The results are: the total number of NS binnaries formed through exchanges of a neutron star in to a binary (Total) and the numbers of LMXBs formed in the simulations – with MS (MS-NS) and RG (RG-NS) donors. The formation rate γ_{ex} calculated from equation 15 (cgs units), is given for LMXBs with MS donors. The other rates can be computed by scaling with the numbers of formed systems. The two groups of columns present results with and without account for stellar collisions.

4.2.1 Monte-Carlo simulations

Theoretically, one could use one of the semi-analytical approximations to the exchange crosssection available in the literature (e.g. Heggie & Hut 1993) and compute the rates from equations 1 and 13. However, the semimajor axis distribution is a function with a complex time evolution, depending on a number of processes and parameters. Another factor, which is even more difficult to account for in an analytical calculation is the effect of mergers during the binary-single interactions. Furthermore, unlike in collisions with red giants and in tidal captures, the binary separation of the exchange binary is large and one would have to take into consideration the subsequent evolution of the binary parameters, before the Roche lobe contact is achieved.

For these reasons we chose to use Monte-Carlo simulations in order to estimate the rate of LMXB formation due to exchange reactions. In these simulations we follow the evolution of binaries in an environment of single stars, with special emphasis on interactions between the single stars and the binaries. The outcome gives a reasonable indication of the importance of this process, compared to the two paths of dynamical formation of LMXBs from single-single encounters discussed above. The simulations are based on the FEWBODY code of Fregeau et al. (2004). FEWBODY numerically integrates the orbits of the stars during the interaction, and automatically classifies and terminates calculations as soon as the outcome is unambiguous, which makes it well suited for carrying out large sets of binary interactions.

All binaries and single stars are assumed to be formed at the same time, and the simulation of the binaries begins 0.5 Gyr after the star formation episode. The masses of single stars are assumed to follow the initial mass function of Kroupa (2001). Only main sequence stars and neutron stars are included, and the main sequence turn-off mass evolves with the age of the population (as given by Girardi et al. 2002). The number density of single stars is kept constant during the simulation.

The initial binaries are drawn randomly from a population with properties typical of binary population synthesis studies. The mass distribution of the primary stars (M_p) was chosen to be the same as the mass function of single stars, while the mass of the secondary chosen from a flat mass ratio distribution. The distribution of orbital separations a was assumed flat in $\log a$ between a minimum separation corresponding to one of the stars filling its Roche-lobe, and a maximum separation of $10^4 R_\odot$. The initial eccentricity of the binaries was set to 0. Each binary is evolved for 15 Gyr in the single star environment, taking into account stellar evolution and evolution of the binary orbit due to magnetic braking and gravitational radiation, as well as encounters with single stars.

The binaries are evolved in timesteps of maximally 0.01 times the average time between encounters with single stars, where an encounter is assumed to happen if a star comes closer than 6 orbital separations. For each timestep binary parameters are adjusted according to gravitational wave emission (Landau & Lifshitz 1962; Peters 1964) and magnetic braking (Rappaport et al. 1983). We assumed the disrupted magnetic braking model, where magnetic braking is ineffective when the MS star is totally convective (Rappaport et al. 1983; Spruit & Ritter 1983). This is the case when the mass of the star is below $\sim 0.4 M_\odot$. The probability of an encounter between the binary and a single star within a timestep of length Δt is given by a weighted average over the distribution of relative velocities and over the mass function of single stars.

$$P_{enc} = \Delta t n_* \int_M \gamma f(M) dM \quad (14)$$

Here n_* is the number density of single stars, γ is given by equation 1, with the cross-section found from equation 3 with $D = 6a$, where a is the orbital separation of the binary. Random numbers are drawn to see whether an encounter occurs. If this is the case, the parameters of the encounter are drawn from their respective probability distributions. The mass of the single star is drawn from the mass function (allowing for neutron stars also). The probability of an encounter distance D is proportional to $\frac{d\gamma}{dD}$ (where σ is given by equation 3) out to the maximum distance of 6 orbital separations of the binary. The distribution of encounter velocities v_{rel} is given by equation 2. The encounter is then solved for using the `binsingle` program of FEWBODY. Binary phase and encounter angle is chosen randomly by FEWBODY from a flat and an isotropic distribution, respectively. The simulation of a binary is terminated when one of the following occurs: (1) the binary is disrupted, (2) one of the stars evolves off the main sequence or (3) Roche-lobe contact is reached. If one of the binary components is an NS, possibility 3 leads to the formation of an LMXB. Possibility 2 also leads to Roche-lobe overflow, but as discussed above, such RGB-NS systems are shortlived and transient X-ray sources.

The simulations are performed with several simplifying assumptions. We discuss the most important of them below. Encounters between binaries are ignored. As most wide binaries are quickly destroyed, the binary fraction decreases fast and binary-binary encounters should only matter at early times. Moreover, in most binary-binary encounters, two or more of the stars merge (Fregeau et al. 2004). Secondly we have neglected the effect of tidal interaction in the evolution of the binaries (Zahn 1989a,b). This will tend to lock the rotation of the stars to the orbit and to circularize the orbit, thus decrease somewhat the time it takes for a system to achieve Roche-lobe contact. The significance of this effect is dif-

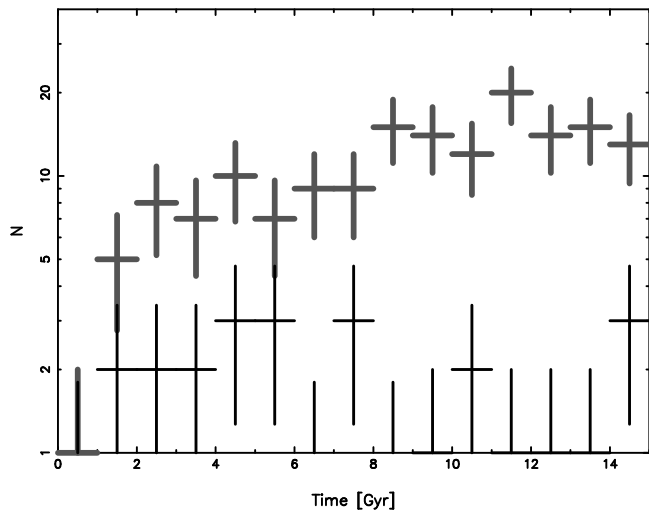


Figure 4. The evolution of the dynamical formation rate of LMXBs due to exchange reactions in a low velocity environment of a globular cluster ($\sigma_v = 15 \text{ km s}^{-1}$). The plot shows the number of systems in which Roche-lobe contact was reached, per time bin, as a function of time from the start of the simulation. Results of simulations without and with account for mergers are shown with thick grey and thin black crosses respectively.

difficult to estimate, for its implementation in population synthesis codes see Belczynski et al. (2005). Evolved stars were not included in the simulations. For the single star population this should not be a problem, as an encounter between an evolved star and a binary will probably lead to a merger of some sort due to the large radius of the evolved star. The net effect of such encounters will most likely be a decreased binary fraction. As for the evolved stars in the binaries, they will lead to Roche-lobe overflow. It is unlikely that a neutron star can be exchanged into such a system without the occurrence of a physical collision. We verified with test simulations that close encounters between tight binaries and single stars in which one of the stars is evolved in almost all cases lead to merger of two or all three stars, in accordance with the conclusions of Fregeau et al. (2004).

4.2.2 Results of simulations

We performed three simulations with different velocity dispersions and densities, to cover the environment in both M31 and in GCs. Parameters and results of the simulations are summarized in table 1. Presented in the table are the numbers of neutron star binaries created in the simulations – the total number and the numbers of Roche-lobe filling systems. The latter is divided into the following two categories: the binaries in which Roche-lobe overflow occurs due to evolution of the binary orbit, while the companion star is on the MS (MS-NS) and the systems in which the mass transfer is initiated due to the evolution of the companion star off the main sequence (RG-NS).

We convert the numbers into γ_{ex} rates, which can be directly compared to the single-single interaction rates computed in the previous section, using

$$\gamma_{ex} = \frac{\Gamma}{n_{bin}n_{ns}} = \frac{N}{T_{sim}n_{ns}N_{bin}} \quad (15)$$

where n_{bin} and n_{NS} are the number densities of binaries and neutron stars, N_{bin} is the total number of binaries in the simulation and T_{sim} is the simulations time span. Note, that with the above definition, N_{bin} is the total number of binaries simulated, i.e. n_{bin} has the

meaning of the primordial volume density of binaries. The rates for MS-NS systems are given in the Table 1. The other rates can be computed from these by scaling according to numbers of binaries. The Monte-Carlo uncertainties can be estimated assuming a Poissonian distribution for the numbers of binaries. In the M31 simulations (the largest value of σ_v) we simulated binaries in a limited range of separations, as wide binaries are quickly ionized and do not contribute to the LMXB production rates. The final value of the exchange rates given in Table 1 has been corrected correspondingly.

In the initial simulations the radii of stars were set to zero, i.e. the possibility of stellar collisions was not accounted for. We performed a second set of simulations, in which two stars with radii R_1 and R_2 were assumed to collide if the distance of closest approach was $D < 1.8(R_1 + R_2)$. We assumed that collisions lead to a merger and removed from simulations all binaries that experience such events. With these assumptions, the rates of LMXB formation decrease dramatically, by about an order of magnitude, i.e. in $\sim 90\%$ of binary-single interactions which could potentially lead to an exchange of the neutron star into the binary, two or more of the stars collide. This result is in agreement with Fregeau et al. (2004) and demonstrates that mergers are a determining factor in the formation of exchange LMXBs.

Figure 4 illustrates the time dependence of the formation rate of exchange LMXBs in a low velocity environment of a typical globular cluster (simulation with $\sigma_v = 15 \text{ km s}^{-1}$). Shown in the figure is the number of binaries per time bin, in which the Roche-lobe overflow was initiated during the given time bin, irrespective of the time when the neutron star was exchanged into the binary. There is an obvious increase with time, due to the fact that in a low velocity dispersion environment most MS-NS binaries are created with relatively large orbital separations and need to be hardened by further collisions in order to become LMXBs. This is in contrast to M31 (large velocity dispersion), where the rate is constant, due to the fact that almost all exchange LMXBs there are formed from binaries with small orbital separations, $a \lesssim 10R_\odot$. For such binaries, binary-single interactions are not an important factor in their further evolution towards Roche-lobe overflow. Also shown in the plot by thin crosses is the result of simulations with account for mergers.

4.3 Comparison of the rates

The results of this section are summarized in figure 5 where we compare the rates for the three main LMXB formation processes, involving neutron stars, as a function of the stellar velocity dispersion. In computing the rates for the tidal capture and collisions with evolved stars we assumed an environment (IMF, age metallicity etc.) similar to the bulge of M31, as described in section 5. The exchange LMXB rates are from the simulations of the previous subsection, without and with account for mergers. It should be noted, that low and high velocity parts of these simulations were tailored for GC and M31 environment respectively, therefore were performed for different values of the stellar density, main sequence cut-off mass M_{co} , age and metallicity. For this reason, although they do correctly illustrate the general trend of the exchange rates with the stellar velocity dispersion, they should not be used to study the exact dependence. One should also keep in mind, that in order to convert the formation rates into the numbers of X-ray sources, the LMXB life-time considerations should be taken into account, as discussed in the section 4.5.

Figure 5 illustrates significant velocity dependence of the relative importance of different LMXB formation channels and

suggests that the relative contributions of different subclasses of LMXBs should be different in GCs and in the galactic centres. In the low velocity environment of a GCs all three processes make comparable contributions to the LMXB production rates (but not to the numbers of X-ray sources observed in any given time, see below), with some prevalence of tidal captures by the main sequence stars, depending on the exact value of the velocity dispersion. In the high velocity environment of a galactic bulge, on the contrary, the tidal capture by main sequence stars with $M_* > 0.4M_\odot$ and exchange reactions are unimportant and the LMXB formation rates are dominated by the collisions with evolved stars and tidal captures by very low mass stars. However, the comparison between globular clusters and M31 is more complex than comparison of the velocity dependent rates, as these environments also differ in other properties of the stellar populations, such as the present day mass function, metallicity, binary fraction etc. This is considered in detail in section 5.

Finally, the total rate of encounters in volume V can be obtained as:

$$R = \int_V \left(\frac{\rho_*}{\langle M \rangle} \right)^2 f \int \gamma(M, M_{ns}, \sigma_v) f(M) dM dV \quad (16)$$

where $f = f_{ns}, f_{bh}, f_{bin}$. Note, that the former two coefficients refer to the present day values, while the latter is the primordial binary fraction, as clarified in the previous subsection.

4.4 Black hole encounters

The discussion above was limited to the formation of LMXBs in which the compact object is an NS. Of course, the same processes are relevant for black holes (BHs), and these are considered below. We assume that stars with initial masses in the $30 - 100M_\odot$ range become BHs, with a canonical mass of $10M_\odot$. The rates of tidal captures and collisions with evolved stars can then be found from the equations of the previous sections, replacing M_{ns} with M_{bh} and f_{ns} with f_{bh} . With the initial mass function of Kroupa (2001), $f_{bh} = 0.17 \cdot f_{ns}$. Note that although there are ≈ 6 times fewer BHs than NSs, this is countered by the gravitational focusing term (equation 3) which makes the encounter cross-section ~ 5 times larger for a BH. As for the neutron stars, we assume that $R_{coll}/R_* = 1.8$. We note, however, that from equation 6 it might be expected that R_{coll} may be larger for the very small mass ratios considered here.

When considering various aspects of single-single encounters on the basis of the total energy arguments it should be noted that the kinetic energy at infinity in the centre-of-masses frame is defined by the reduced mass $\mu = M_1 M_2 / (M_1 + M_2)$ which, for the low mass stars, only depends weakly on the compact object mass. Therefore, even if the energy equipartition is inefficient and the NS and BH velocity dispersions are comparable, as is the case in the M31 bulge, the kinetic energy at infinity, $\mu v_{rel}^2 / 2$, will not be much higher in the case of a black hole.

For this reason the energy considerations in collisions with evolved stars (section 4.1.1, eq.7), will not change significantly and the fraction of collisions expected to lead to a bound systems for a given velocity dispersion depends only weakly on the mass of the compact object.

For tidal captures, the energy of the oscillations induced in the non-degenerate star is roughly $\propto M_{NS,BH}^2$ (see equation 9), and the capture distance is therefore larger for BHs than for NSs. At low velocities, this can enhance the rate by a moderate factor of ~ 2 . At large velocities, on the contrary, $R_{tid} \sim R_{coll}$, and even a small

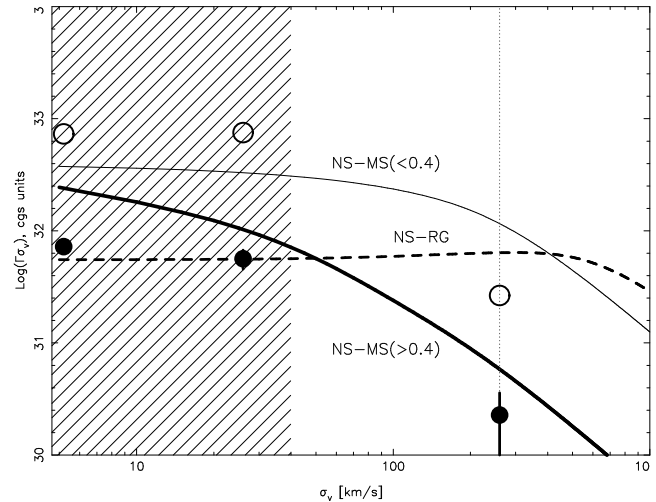


Figure 5. Comparison of NS LMXB dynamical formation rates as a function of the stellar velocity dispersion. Shown are the rates $\gamma\sigma_v$ for tidal captures by main sequence stars $> 0.4M_\odot$ (thick solid line) and $< 0.4M_\odot$ (thin solid line), collisions with evolved stars (assuming $\lambda\eta = 0.5$, dashed line) and exchange reactions (circles with error bars). For the exchange reactions, results are shown for simulations without (open symbols) and with (filled symbols) account for collisions. Error bars are only shown if they are larger than the circles. The hatched area shows the velocity dispersion range typical for globular clusters, the dotted line for the inner bulge of M31.

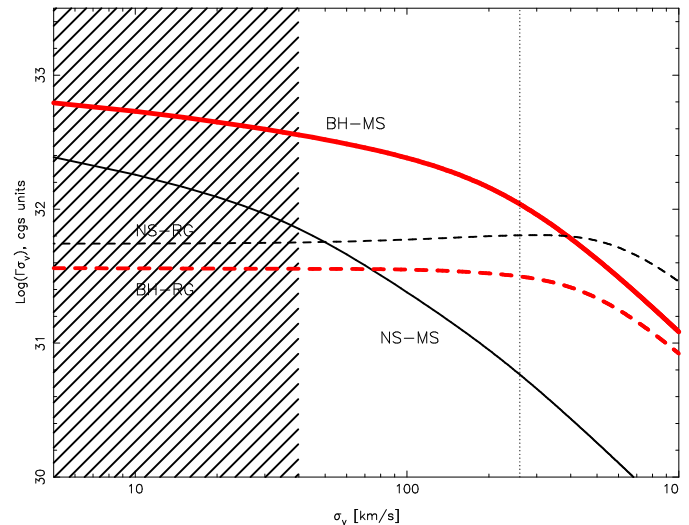


Figure 6. Comparison of the LMXB formation rates in encounters with neutron stars (thin lines) and black holes (thick lines). Shown are tidal captures by main sequence stars of mass $> 0.4M_\odot$ (solid lines) and collisions with RGB/AGB stars (dashed lines). The normalization of the BH rates have been multiplied with f_{bh}/f_{ns} .

increase in R_{tid} can drastically increase $\sigma_{tid} - \sigma_{coll}$ and thereby the overall tidal capture rate. As the total energy to be dissipated in the interaction depends weakly on the compact object mass, the impact of the tidal oscillation on the thermal state of the normal star does not become more severe for the black hole. Therefore, if a tidal capture is possible at all, it is possible for black holes as well as for neutron stars.

There is one important difference between BHs and NSs, namely that the retention factor for black holes in globular clusters is close to zero (O’leary et al. 2006). For this reason, black holes

do not contribute to dynamical LMXB formation in globular clusters. In M31, however, the black hole fraction should be close to the IMF-based estimate given above, due to much longer energy equipartition time scale than in globular clusters.

In figure 6 we compare the LMXB formation rates in single-single encounters involving black holes and neutron stars. Obviously, black holes can make sizable contribution to the LMXB formation rates, especially in the high velocity regime.

4.5 Numbers of X-ray sources

In order to convert the encounter rates to the numbers of X-ray sources observed at any given moment of time, one needs to consider the evolution of a binary through the X-ray phase. A definitive answer can be obtained from proper population synthesis calculations, which is beyond the scope of this paper. In a simpler approach one may consider characteristic life times τ_X of binaries at different phases of its evolution. The number of X-ray sources N_X can be then related to the corresponding encounter rate: $N_X \sim \gamma \tau_X$. Taking into account dependence of the τ_X on the mass and evolutionary status of the donor star and their mass distribution, we obtain an expression, similar to the equation 16 for overall encounter rate:

$$N_X \approx \int_V \left(\frac{\rho_*}{\langle M \rangle} \right)^2 f \int \tau_X(M) \gamma(M, M_{ns}, \sigma_v) f(M) dM dV \quad (17)$$

where f is defined as in eq.(16) and $\tau_X(M) = \Delta M_d / \dot{M}$, $\Delta M_d = M_i - M_f$, M_i is the initial mass of the donor star and M_f its final mass in the given evolution stage (e.g. for a star with initial mass $> 0.4M_\odot$, $M_f = 0.4M_\odot$ – the mass corresponding to the period gap). In case of an LMXB powered through the Roche-lobe overflow, the \dot{M} is defined by the orbital braking mechanism and the mass-radius relation for the donor star. The stability of the mass transfer in the accretion disc should be also taken into account in order to identify persistent/transient nature of the binary. The integral in eq.(17) is taken over the range of the masses relevant to the given type of X-ray binaries.

Below we examine evolution and characteristic values of \dot{M} of X-ray binaries formed via different dynamical processes considered in in this paper. We accept the standard prescriptions for the magnetic braking (Rappaport et al. 1983) and gravitational radiation (Landau & Lifshitz 1962; Peters 1964) and the transiency criterium in the form published by Dubus et al. (1999) for irradiated discs. One should keep in mind that these simple prescriptions predict time averaged quantities but may fail to explain the momentary values of luminosity, which may vary significantly on the timescales of days–months–years. The dependences of the mass accretion rate on the mass of the donor star for NS and BH binaries are shown in figure 7. These dependences were computed based on standard formulae for a Roche lobe filling secondary (van den Heuvel 1992) assuming that the secondary is in the thermal equilibrium. As was demonstrated by Stehle et al. (1996), this assumption gives sufficiently accurate results for the main sequence donor. For the mass-radius relation we used the 10 Gyr isochrones of Baraffe et al. (2003) and Baraffe et al. (1998) for stars $M < 0.1M_\odot$ and $M > 0.1M_\odot$, respectively. Also shown in figure 7 are transiency limits for different types of compact object. The NS and BH masses were assumed 1.4 and 10 M_\odot respectively. The spike in \dot{M} at $\approx 0.07M_\odot$ is caused by the shape of mass-radius relation near the end of the nuclear burning, as given by the isochrones. It is less pronounced in the 1 Gyr isochrones (shown in figure 7 by thin solid lines) which might be more appropriate for the thermal state of a mass-losing brown dwarf. We did not investigate the reality of this

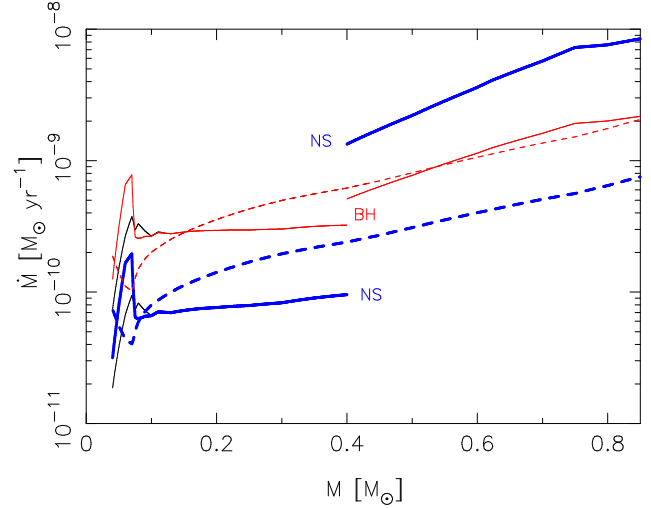


Figure 7. Dependence of the mass accretion rate \dot{M} in a Roche-lobe filling system on the mass of the donor star. The curves for a neutron star and a black hole binary are shown by thick and thin lines. The calculations based on 10 and 1 Gyr isochrones give identical result down to $\sim 0.1M_\odot$, below which the 10 Gyr isochrones give more pronounced spike in \dot{M} . The transiency limits are plotted by respective dashed lines. The method of calculations and assumptions are described in section 4.5

spike and note, that its presence or absence does not significantly affect our conclusions.

Collisions with evolved stars. In a collision with a red giant, an ultra-compact X-ray binary (UCXB) with a He white dwarf donor is formed. The white dwarf mass equals approximately the mass of the red giant’s core (Lombardi et al. 2006), i.e. is in the 0.1-0.4 M_\odot mass range, depending on the evolutionary stage of the red giant. The evolution of such a system includes a very fast initial stage of very short, \sim minutes, orbital period and very high, super-Eddington \dot{M} . During this period the white dwarf donor is quickly reduced to a $\sim 0.06M_\odot$ after which a more “normal” UCXB with $P_{orb} \sim 10$ min and $L_X \sim 10^{38}$ erg/sec emerges, similar to the ones observed in our Galaxy. Overall, such a system will spend ~ 0.1 Gyr with the luminosity $10^{36} - 10^{38}$ erg/sec, before the white dwarf is depleted below $\approx 0.02M_\odot$. Somewhere around this mass the sources will cross the stability threshold and will become transient (Deloye & Bildsten 2003; Bildsten & Deloye 2004).

The cores of less evolved, sub-giant stars are not fully degenerate and/or hydrogen-depleted. In this case a collision will result in a binary with He or brown dwarf donor, depending on the core mass and chemical composition. Such a binary is also driven by gravitational radiation, but due to the larger radius the period minimum is higher, $\sim 20 - 30$ minutes, and super-Eddington mass transfer does therefore not occur. For such systems, a life time of $\sim 200 - 300$ Myrs may be expected (N.Ivanova, private communication). In order to make a crude estimate of their fraction we assume that the core of an RGB star becomes fully degenerate, when the central density exceeds $\rho_c \approx (5 - 10)\rho_{crit}$, where ρ_{crit} is the critical density above which electron gas is degenerate ($\rho_{crit} \sim 2.4 \cdot 10^{-8} \mu_E T^{3/2}$ g cm $^{-3}$). We estimated from the Padova stellar tracks that this occurs at stellar radii of $R \sim (3 - 5) \times R_\odot M/M_\odot$. As discussed in section 4.1.1, given the high stellar velocities in M31, only RGBs with rather small radii can effectively capture a compact object through collisions, and we expect that in a large fraction, $\sim 50 - 80$ per cent, of X-ray sources created through this mechanism the donor star is

not fully degenerate. In the low velocity environment of globular clusters this fraction is smaller, $\sim 25 - 40$ per cent.

Tidal captures by main sequence stars with $M > 0.4M_{\odot}$ lead to formations of “usual” LMXBs, similar to the ones constituting the majority of systems with main sequence donors observed in the Galaxy. These sources are driven by the magnetic braking and luminosities of $\sim 10^{36.5-38.0}$ erg/sec and lifetimes of $\sim 0.1 - 0.5$ Gyr should be expected. Note, that these estimates depend critically on the magnetic braking prescription, the weak magnetizing breaking predicting up to several times smaller luminosities and longer life times (Ivanova & Kalogera 2006). All black hole systems are expected to be transient, in agreement with BH binaries statistics in the Milky Way.

Tidal captures by main sequence stars of very low mass, $M < 0.4M_{\odot}$. For these fully convective very low mass stars the magnetic braking is believed to be inefficient, therefore the accretion is driven by the gravitational radiation. Given that the orbital periods of these systems are in the \sim hours range, gravitational radiation can provide luminosities of $\sim 10^{36.0-36.5}$ and $\sim 10^{36.5-37.0}$ erg/s for NS and BH systems respectively. The systems with $M \lesssim 0.15M_{\odot}$ will be transient, these constraints being more severe for the NS binaries. The life times during the persistent phase are ~ 300 Myr. The life times during the transient phase are ~ 1 and ~ 4 Gyrs for BH and NS systems respectively.

It is interesting to consider the final stage of evolution of these systems, after the donor star is reduced to $\sim 0.1M_{\odot}$, below the nuclear burning limit. As these are descendants of very low mass stars, whose nuclear time scale is much longer than the cosmological time, they will become brown dwarfs of mass $\sim 0.05M_{\odot}$. Given the mass-radius relation for brown dwarfs, the M drops quickly (Fig.7) and these systems become transients, similar to some of the accreting msec pulsar systems, observed in our Galaxy.

We note that in the binary systems with very low mass ratios, $q \lesssim 0.02$, the circularization radius exceeds the tidal truncation radius (e.g. Paczynski 1977). It is therefore not entirely clear whether the stable mass transfer is possible, see e.g. discussion in Yungelson et al. (2006) (section 3.3). Such low mass ratios can be reached for the most low mass black hole systems.

5 M31 AND THE MILKY WAY GLOBULAR CLUSTERS

Below we compute rates of dynamical formation of LMXBs and their expected numbers in M31 and in Galactic GCs. For this, we need to specify velocity dispersion, initial and present day mass functions, age, metallicity and stellar isochrones. These parameters are different in GCs and galactic centres. The difference in stellar velocities is an important one, as discussed in section 4.3, but several other properties of stellar populations play equally significant roles in shaping the population of dynamically formed binaries. The factor of prime importance is highly efficient mass segregation in GCs. Its two most significant consequences are:

(i) The present day mass function. Due to efficient mass segregation, the inner regions of the GCs, where most of the encounters happen, are depleted of low mass stars, to the degree that the mass function is essentially flat (e.g. King et al. 2005; de Marchi & Paresce 1997; Albrow et al. 2002). This is not the case for a galactic bulge, where the mass distribution of main sequence stars is sufficiently well represented by the Kroupa IMF (Zoccali et al. 2000). As a result, the tidal captures by very low mass stars, dominating the binary formation processes in M31 (Fig.5), are significantly less important in GCs.

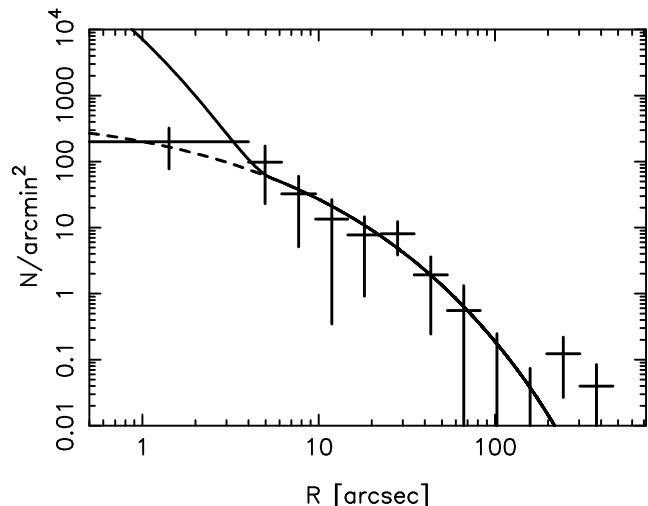


Figure 8. The radial distribution of “surplus” X-ray sources computed as a difference between the data and best fit model in figure 1. The solid line shows the projected ρ_*^2 distribution, computed from the original mass model of the M31 bulge from Riffeser et al. (2005). The dashed line was computed from the mass distribution with the circumnuclear stellar disc excluded. Both model distributions are normalized to the observed number of surplus sources outside 4 arcsec.

(ii) Abundance of BHs. GCs are believed to be completely depleted of black holes (O’leary et al. 2006), due to mass segregation and BH-BH encounters. Therefore tidal captures of BHs do not play any roles in globular clusters as opposite to the case of M31. Note that in the latter case the role of black holes is further enhanced by the velocity dependence of the tidal capture cross-section, as discussed in section 4.4 and shown in figure 6.

Among other factors, leading to further quantitative differences, the following should be mentioned: (i) Due to supernova kicks, large fraction of neutron stars escape the parent cluster, with the NS retention factor being in the $\sim 0.1 - 0.2$ range (Pfahl et al. 2002). On the other hand, the mass segregation of the remaining NSs may increase their density near the globular cluster centres, thus compensating for the low retention fraction. (ii) Binary fractions are different in globular clusters and galactic centres, due to different rates of binary-single processes, caused by difference in velocities and stellar densities. This is important for exchange rates and is taken into account in our simulations automatically. (iii) Finally, different ages and, especially metallicities result in different mass-to-light ratios, the main sequence turn-off mass and duration of the red giant phase, as discussed in section 5.2.

For these reasons the comparison between globular clusters and M31 is more complex than comparison of the velocity dependent rates, shown in figure 5. It is the subject of this section.

5.1 M31

For the stellar models we used an ischrone with a metallicity ~ 1.5 times solar and an age of 12 Gyr (isochrone file isoc_z030.dat from Girardi et al. 2002). This gives a main sequence turn-off mass of $0.9532 M_{\odot}$ and a mass at the tip of the AGB of $1.0081 M_{\odot}$ (initial masses). Stars more massive than this have all turned into stellar remnants.

The velocity dispersion (3D) was assumed to be constant,

Object (1)	Type (2)	MS(< 0.4M _⊙) (3)	MS(> 0.4M _⊙) (4)	RGB (5)	HB (6)	AGB (7)	Exchange (8)
NS	Tidal capture	15.1 (15.7)	0.8 (0.9)	0.01	-	-	3.5
NS	Collisions	36.6	46.6	6.5-13.3	5.2	0.01-0.67	0.3
BH	Tidal capture	65.3 (65.3)	14.2 (14.2)	0.09	-	-	8.8
BH	Collisions	37.7	38.0	3.1-5.8	2.0	0.00-0.06	1.0

Table 2. Formation rates of LMXBs in M31, per Gyr. The entries in bold are expected to lead to the formation of LMXBs. The columns are: (1) The type of compact object; (2) the capture process; (3) rate of interactions with MS stars of mass < 0.4M_⊙, only those initiating Roche-lobe overflow within 5 Gyr are included (full number is given in the parenthesis); (4) rate of interactions with MS stars of mass > 0.4M_⊙, same criteria as (3); (5) rate of interactions with stars on the RGB, for collisions only those with $a_f < 5R_⊙$ are included for $\eta\lambda = 0.1 - 1.0$; (6) rate of interactions with stars on the HB, tidal captures were not calculated; (7) rate of interactions with stars on the AGB, tidal captures were not calculated, same criteria as (5); (8) LMXBs created through exchange reactions, estimated from simulations without collisions (in tidal capture rows) and with collisions (in collision rows).

$\sigma_v = 260 \text{ km s}^{-1}$ (McElroy 1983; Widrow et al. 2003). The density structure of M31 was constructed using the model of Riffeser et al. (2005), based on the Gunn-r band photometry presented by Kent (1989). In this model the total R-band luminosity of the bulge out to a distance of 12 arcmin from the centre of M31 is $1.18 \cdot 10^{10} L_{\odot,R}$. We normalized the density by requiring the integrated R-band luminosity over the mass function (giving a mass-to-light ratio of $(M/L)_R = 3.27$) to match the R-band luminosity of the model, giving the bulge a total mass of $3.9 \cdot 10^{10} M_{\odot}$ of stars in the 0.1-1.0081 M_{\odot} range. The projection of this model agrees with the mass distribution inferred from the K-band light, which was used to model the LMXB distribution in Voss & Gilfanov (2007). The observed K-band luminosity of the region is $4.4 \cdot 10^{10} L_{\odot,K}$, and integrating over the isochrone, we find a mass-to-light ratio of $(M/L)_K = 0.76$, giving a total mass of $3.4 \cdot 10^{10} M_{\odot}$, compatible with the R-band estimate. As a consistency check, we estimate the mass, using the mass-to-light ratios of Bell & de Jong (2001). With the bulge colour $(B-V) = 0.95$ (Walterbos & Kennicutt 1987), we find a bulge mass of 3.75 and $3.73 \cdot 10^{10} M_{\odot}$ from the R-band and the K-band, respectively.

In figure 8 the ρ_*^2 profile, integrated over the line of sight, is compared to the observed distribution of surplus sources, which was calculated by subtracting the best-fit model of LMXBs and CXBs from the observed radial distribution of X-ray sources (section 2, figure 1). It is obvious that the distributions agree well everywhere outside ~ 4 arcsec. In the innermost 4 arcsec of M31 the mass model of Riffeser et al. (2005) features a sharp increase in density, absent in the distribution of X-ray sources. This increase is due to a stellar disc of high density surrounding the central supermassive black hole (Bender et al. 2005). In this paper we do not try to model the environment in this region and exclude the disc component. The stellar model used for computation of the encounter rates is described by the following distribution:

$$\rho_{bulge} = \rho_0 10^{-0.4(7.1a_{bulge}^{1/4} + 0.61)} \quad (18)$$

where

$$a_{bulge} = \frac{0.254z_0^2 + \sqrt{0.254^2 z_0^4 + 4(x_0^2 + y_0^2 + 1.11)z_0^2}}{2} \quad (19)$$

with a_{bulge} , x_0 , y_0 and z_0 expressed in arcmin. The inclination of the bulge coordinate system is assumed to be 77° , and $\rho_0 = 4.34 \cdot 10^4 M_{\odot} \text{ pc}^{-3}$ (using our mass to light ratio $(M/L)_R = 3.27$). This gives a bulge mass (within 12 arcmin from the centre) of $3.87 \cdot 10^{10} M_{\odot}$ and

$$\int \rho_*^2 dV = 4.6 \cdot 10^{11} M_{\odot}^2 \text{ pc}^{-3} \quad (20)$$

It is now straightforward to calculate the rates of tidal captures and collisions. Following the equations of section 4 the rates are given by

$$R_{M31} = \int_{bulge} \left(\frac{\rho_*}{\langle M \rangle} \right)^2 dV \cdot f_{ns} \int_{M_{low}}^{M_{high}} f(M) \gamma dM \quad (21)$$

where $M_{low} - M_{high}$ is the initial mass range for the type of stars for which the rates are calculated. The rates for different types of encounters are summarized in Table 2. For clarity the channels expected to lead to the formation of LMXBs are written in bold font.

5.1.1 Numbers of X-ray sources

We turn now to the numbers of dynamically formed X-ray sources. As it is obvious from Table 2 (column 4), the number of “normal” persistent LMXBs with a neutron star accreting from a main sequence companion $M_* > 0.4M_{\odot}$, which constitute the majority of the primordial LMXBs, is negligibly small (BH capture products with $M_* > 0.4M_{\odot}$ donors are expected to be transients and are discussed below). The two main contributions to the population of dynamically formed sources come from the tidal captures of black holes and neutron stars by very low mass MS stars, and from collisions of compact objects with RGB stars (columns 3 and 5). In computing the numbers of sources from equation 17 we take into account that the evolutionary timescales of all types of dynamically formed X-ray sources are much shorter than the life time of the bulge. Therefore the systems formed via tidal capture by $M_* > 0.4M_{\odot}$ stars will pass through the phase of the very low mass companion in the end of their life time, adding to the numbers of persistent and transient sources of this type. Similarly, a capture product of, for example, a $0.3M_{\odot}$ star will go through the transient phase in the beginning of its X-ray active phase and will become a persistent source after the donor star is depleted below $\sim 0.10 - 0.15M_{\odot}$. We thus predict ~ 24 and ~ 5 persistent X-ray sources with black holes and neutron stars respectively, accreting from the very low mass stars. To this number should be added the number of ultra-compact X-ray binaries produced via collisions of compact objects with red giants, which is ~ 3 . The total number of predicted persistent sources is compatible with, albeit somewhat larger than the observed number of surplus sources, ~ 21 . Given the number and magnitude of uncertainties involved in the calculations and the simplifications made, we consider this as a good agreement.

Based on the range of the donor masses corresponding to unstable mass transfer (figure 7), we predict ~ 30 BH and ~ 22 NS transient sources with very low mass donors $M_* < 0.4M_{\odot}$, as

Metallicity	Type	MS(< 0.4M _⊙)	MS(> 0.4M _⊙)	RGB	HB	AGB	Exchange
0.2 solar	Tidal capture	12.9 (17.2)	24.8 (25.7)	7.0	-	-	203.4
	Collisions	10.5	51.3	24.3-27.7	4.6	0.4-1.1	15.3
0.02 solar	Tidal capture	8.6 (10.8)	14.3 (14.7)	2.9	-	-	117.3
	Collisions	6.6	28.6	10.1-11.7	2.0	0.3-0.6	8.8

Table 3. Total encounter rates for 140 Galactic globular clusters from Harris (1996) for which sufficient structural parameters are known, calculated assuming metallicity of 0.2 and 0.02 solar. Entries in bold indicate paths expected to lead to the formation of LMXBs. The rates are given in LMXBs/Gyr. These 140 GCs contain the 13 LMXBs observed in the Galactic GC system. The notation is the same as in table 2

Population	LMXBs observed	Type	MS(< 0.4M _⊙)	MS(> 0.4M _⊙)	RGB	HB	AGB	Exchange
Red GCs	8	Tidal capture	4.1 (5.2)	6.5 (6.7)	1.6	-	-	53.3
		Collisions	3.4	16.8	7.9-9.2	1.5	0.1-0.4	4.0
Blue GCs	5	Tidal capture	5.9 (7.6)	10.5 (10.8)	2.2	-	-	86.1
		Collisions	4.4	19.2	6.8-7.8	1.3	0.2-0.4	6.5

Table 4. Total encounter rates calculated separately for red and the blue Galactic globular cluster subsystems, assuming metallicity of 0.2 and 0.02 solar respectively. Bold entries indicate paths expected to lead to formation of LMXBs, and the rates are given as LMXBs/Gyr. The notation is the same as in table 2.

well as ~ 3 BH transient sources with MS donors $> 0.4M_{\odot}$. Furthermore, exchange reactions might contribute with a number of LMXBs with RGB donor stars, that are also transient, but duration of their active phase is restricted by the life time of the red giant donor. The number of transients observed at any given moment in time depends on their duty cycle. Taking Galactic black hole transients with the main sequence donor as an example, one could expect a duty cycle of $\sim 1/50$, giving one bright transient in ~ 15 years. As for the transients with very low mass donors, one can use the accreting msec pulsars as an example of NS systems. SAXJ1808.4-3658 has outbursts lasting for $\sim 2-3$ weeks every ~ 2 years, and the duty cycle is therefore ~ 0.03 . Assuming crudely that it is the same for BH and NS systems, we would expect 1.5 transient sources at any given time. The outbursts of accreting msec pulsars in our Galaxy are characterized by low peak luminosities, $\log(L_X) \sim 36 - 36.5$. Therefore many, if not most, of outbursts from these sources will be missed in a Chandra survey of the type reported in Voss & Gilfanov (2007) which detects mostly brighter transients, with the peak luminosity of $\log(L_X) \gtrsim 36.5$. This explains why Voss & Gilfanov (2007) have not found any excess in the number of transient sources close to the galactic center – the fraction of transients detected inside 1 arcmin from the center (5 out of 28 in 29 Chandra observations with the time span of ~ 5 years) agrees with the fraction of stellar mass contained in this region. On the other hand Chandra observations of our Galactic Center, having much better sensitivity, have indeed revealed overabundance of faint transients (Muno et al. 2005).

5.2 Globular Clusters

Due to high efficiency of the mass segregation in globular clusters the (retained) neutron stars will be much more centrally concentrated than low mass stars. Assuming that stellar density and velocity dispersion are approximately constant over the region occupied by the neutron stars, one can approximately write:

$$\int_V n_{ns} n_* \Gamma dV \approx n_* \Gamma \int_V n_{ns} dV = k N_{ns} n_* \Gamma \quad (22)$$

where N_{ns} is the total number of neutron stars in the globular cluster under consideration, n_* is the central density of stars and $k \sim 1$ is a constant accounting for inaccuracy of this approximation. Assuming that the distribution of normal stars follows the analytic King model (Lugger et al. 1995; Grindlay et al. 2002), and that the NSs are in thermal equilibrium with the stars at turn-off ($0.80-0.85 M_{\odot}$), we estimated that $k \sim 0.2 - 0.3$. Total thermal equilibrium is generally not reached, the value of k is therefore slightly lower. In the following we will use a value of $k = 0.2$ for all globular clusters.

We use the catalogue of Harris (1996) for the globular clusters parameters required to estimate the formation rates of LMXBs in the Galactic GCs. Of the 150 GCs included in the catalogue, the parameters are missing for 10, and we ignore these. The stellar populations in the GCs were modelled using the isochrones of Girardi et al. (2002), with an age of 11 Gyr (Salaris & Weiss 2002). The N_{ns} for each GC was computed as follows. Assuming the initial mass function of Kroupa (2001), we used the integrated light of the isochrones to compute the present day mass-to-light ratio and from the total V-band luminosity of the GCs computed the IMF normalization. Assuming further that all stars with the initial mass in the range of $8 - 30 M_{\odot}$ have become neutron stars and retention factor of 10 per cent (Pfahl et al. 2002) we finally compute the present day number of the neutron stars in each globular cluster, N_{ns} . On the other hand, we assumed that the present day mass function in the GC centers is flat. With this mass function we again use the integrated V-band light of the isochrones to calculate n_* from the V-band luminosity density ρ_V given in Harris (1996). For the 56 GCs in Pryor & Meylan (1993) we use their central velocity dispersions v_0 needed to compute the encounter rates. The remaining GCs were dealt with as follows. From the virial theorem we expect that $v_0 \sim K r_c \sqrt{\rho_0}$, where r_c is the core radius of the GCs, and ρ_0 is the central density; we further assumed that $\rho_V \propto \rho_0$. We performed the least square fit to the known central velocity dispersions in 56 GCs and found $K = 0.18 \text{ km s}^{-1}$ and 0.17 km s^{-1} for the metal-rich and metal-poor GCs respectively (assuming that r_c is in pc and ρ_V in $M_{\odot, V} \text{ pc}^{-3}$). These values have been used to find v_0 for the remaining 84 GCs.

5.2.1 Metallicity effects

In order to study the metallicity dependence of the encounter rates, we compute the cumulated rates for two metallicities, 20 per cent, and 2 per cent of the solar value (files `isocz004.dat` and `isocz0004.dat` from Girardi et al. (2002)) which are representative of the red and blue GC populations, respectively. The results are presented in table 3 and show a ~ 1.5 - 2.5 increase in the encounter rates for the higher metallicity case.

The metallicity dependence in our calculations is mainly due to two factors. (1) As noted by Bellazzini et al. (1995) the radii of metal-rich stars are larger, and therefore the rates of tidal captures and collisions are higher. Furthermore the duration of the RG phase is longer for metal-rich stars. As demonstrated by Maccarone et al. (2003) this effect can maximally lead to an enhancement of the cross-sections and rates by ~ 60 per cent, and most likely ~ 30 per cent. Our results are consistent with this, showing a ~ 20 per cent increase in tidal captures by MS stars ($> 0.4M_{\odot}$) and ~ 50 per cent increase in collisions with RGB/AGB stars. For exchange reactions the effect is negligible. (2) Theoretical isochrones predict that the V -band mass-to-light ratio of the metal-rich population is higher than that of the metal-poor population. As the stellar densities are given in Harris (1996) in the form of V -band luminosity density, the encounter rate is proportional to $\rho_*^2 \propto (M/L)^2$. This could result in an additional ~ 60 per cent increase in the rates. It is however unclear, whether this is the case for real globular clusters – observations indicate that the central mass-to-light ratio might be independent on the metallicity (McLaughlin 2000). This could be due to the fact that the red GCs typically are more dynamically evolved (but not older) than the blue ones and therefore have a flatter mass function in their cores (McClure et al. 1986; Vesperini & Heggie 1997; Piotto & Zoccali 1999). Moreover, these structural differences may be the true reason for the observed metallicity dependence of the abundance of dynamically created sources in globular clusters as also noted by Bregman et al. (2006).

Thus our calculations do indicate a moderate metallicity dependence of the encounter rates. It is however insufficient to explain observations. Indeed, there are ~ 3 times as many LMXBs in red GCs as in blue GCs of the same size in the Galaxy (Grindlay 1993; Bellazzini et al. 1995), where 8 out of 13 LMXBs are observed in the red GC system containing 46 out of the total number of 140 GCs with known metallicities (assuming a division at $[\text{Fe}/\text{H}]=-1$). Similar trend is observed in in other galaxies (Kundu et al. 2002; Sarazin et al. 2003; Kim et al. 2006).

5.2.2 Predicted rates and numbers of X-ray sources

To predict the total rates of LMXBs formation in the Galactic GCs, we divide the GCs into two subpopulations depending on metallicity, red (46 GCs) and blue (94 GCs). The cumulative rates for these two subpopulations are then calculated as above, assuming all red GCs to have 0.2 solar metallicity and all blue ones to have 0.02 solar metallicity. The results are given in table 4. As it can be expected from figure 5, all three processes give comparable contributions.

For metal-rich clusters, these rates predict ~ 0.5 X-ray binaries with the companion mass $> 0.4M_{\odot}$ due to tidal captures, with an additional $0.5-1.0$ such binaries from exchange reactions, ~ 1.5 UCXBs and ~ 3 fainter LMXBs with very low mass companion. Corresponding to ~ 6 sources overall, this is in a good agreement with the total number of LMXBs observed in metal-rich clusters (8). On the other hand, we do overpredict the numbers of X-rays sources in the metal-poor GCs by a factor of ~ 1.5 – although

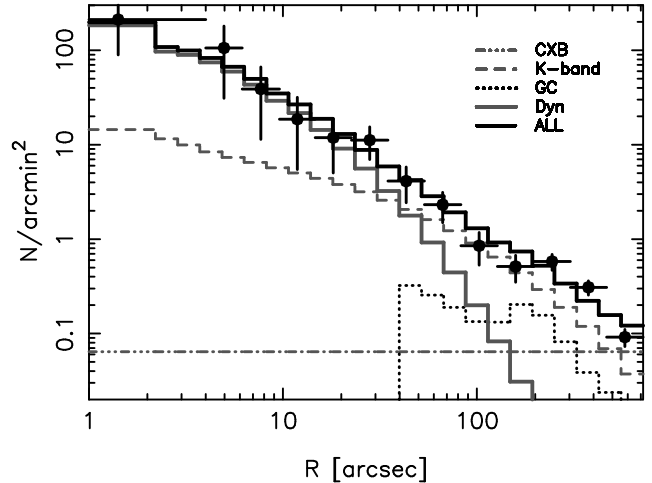


Figure 9. The observed radial distribution of the X-ray sources in the bulge of M31, compared with the expected contributions of different subpopulations of low-mass X-ray binaries: primordial, binaries in globular clusters and binaries formed through dynamical interactions in the inner bulge of M31. The dash-dotted horizontal line shows contribution of the background AGN. The total numbers of sources are summarized in table 5.

Type	Number
Background sources	29
Primordial LMXBs	64
LMXBs in globular clusters	21
LMXBs dynamically formed in the bulge	21

Table 5. Numbers of X-ray sources of different origin in the bulge of M31, $r < 12$ arcmin, $L_X > 10^{36}$ erg/s

our calculations do show the expected metallicity dependence, it is compensated by the larger number of metal-poor clusters. Note that the number of bright sources with $M_d > 0.4M_{\odot}$ main sequence companion depends critically on the rate of magnetic braking. The above numbers have been computed with the standard prescription of Rappaport et al. (1983). The weaker variants of magnetic braking (e.g. Ivanova & Taam 2003) may give upto a factor $\sim 5-10$ longer lifetimes and, consequently, larger numbers of LMXBs with $M_d > 0.4M_{\odot}$ donors. This can change the overall numbers for globular clusters, but is insignificant factor in the M31 bulge calculations, due to negligible contribution of these systems there.

It is interesting to compare the numbers of ultra-compact systems. Considering metal rich clusters only, 2 of the 8 LMXBs have measured orbital periods < 1 h and are therefore most likely UCXBs (Benacquista 2006). Of the 6 others 4 have undetermined periods and could therefore be either UCXBs or traditional LMXBs. The final 2 have orbital periods > 5 h. Thus, there may be from 2 to 6 short period systems. We predict ~ 1.6 UCXBs formed in the collisions with red giants. In addition, the LMXBs with the very low mass donor stars, $M_d < 0.15M_{\odot}$, for which the predicted number is ~ 2.4 , will also have short orbital periods and faint optical counterparts and may contribute to the observed statistics of UCXBs, giving a prediction of ~ 4 short period systems in total.

6 CONCLUSIONS

We have studied the spatial distribution of the luminous X-ray point sources ($L_x > 10^{36}$ erg s $^{-1}$) in the bulge of M31. We show that there is a significant increase in the specific frequency of sources, per unit stellar mass, in the inner ≈ 1 arcmin. This behaviour is similar, although smaller in the magnitude, to that observed in globular clusters. The radial distribution of the surplus sources follows the ρ_*^2 profile. All these suggest that the surplus sources are dynamically created in stellar encounters in the high stellar density environment of the inner bulge of M31. This is further confirmed by the peculiarity of their luminosity distribution, which resembles that of the globular cluster sources in M31 and our Galaxy (Voss & Gilfanov 2007).

It has long been known that dynamical interactions are responsible for the relatively large number of X-ray sources observed in globular clusters, but this is the first evidence of the dynamical formation of LMXBs in the vicinity of a galactic center. The stellar velocities in bulges are higher than in globular clusters by a factor of $\sim 5 - 10$. We therefore performed a detailed study of the velocity dependence of the three main dynamical processes leading to the formation of LMXBs: tidal captures of a compact objects by main sequence stars, collisions between evolved stars and compact objects and the exchange of a compact object into an already existing binary. Another major factor affecting the overall encounter rates and the numbers of dynamically formed LMXBs is the high efficiency of the mass segregation in globular clusters, which modifies significantly the spatial distributions of objects of different mass and affects the present day mass function in different parts of a globular cluster. In addition, due to the relative shallowness of the potential well, the populations of compact objects are significantly depleted in globular clusters.

We found that while exchange reactions are potentially the dominant formation channel in globular clusters (although stellar collisions might decrease the importance of this channel significantly), this process is relatively unimportant in M31. Similarly, tidal captures of NSs by main sequence stars of mass $> 0.4M_\odot$ are important in globular clusters, but not in M31. Instead the main formation channel is tidal captures of compact objects by low mass ($< 0.4M_\odot$) stars, with some contribution from collisions between red giants and compact objects. While the geometrical collision rate is high enough to explain the total number of sources from the latter channel, the majority of the collisions are unlikely to lead to the formation of a binary system, as the binding energy of the envelopes of most RGB/AGB stars is too low to capture a compact object in a high velocity environment. We conclude that the majority of the sources in M31 are short-period binaries, and in contrast to globular clusters many of them have BH accretors. We note that the BH binaries with a very low mass companion may become persistent X-ray sources after the donor star is depleted below, $M_d \lesssim 0.15M_\odot$, due to small size of the accretion disc and the positive dependence of the gravitational breaking rate on the mass of the primary. We also predict for M31 a large number of faint transients, similar to the accreting msec pulsars in our Galaxy. Overall, we have been able to explain the spatial distribution and absolute numbers of surplus sources detected in the inner bulge of M31 as well as the statistics of LMXBs in the metal rich globular clusters. However, we overpredict by a factor of ~ 1.5 the population of LMXBs in the metal poor clusters.

Finally, the sub-populations of low-mass X-ray binaries in the bulge of M31 are summarized in Fig.9 and Table 5.

Acknowledgements The authors would like to thank Natasha Ivanova for numerous discussions and useful comments on the initial version of the manuscript.

REFERENCES

- Albrow M. D., De Marchi G., Sahu K. C., ApJ, 579, 660
 Baraffe I., Chabrier G., Barman T. S., Allard F., Hauschildt P. H., 2003, A&A, 402, 701
 Baraffe I., Chabrier G., Allard F., Hauschildt P. H., 1998, A&A, 337, 403
 Barmby P., Huchra J. P., 2001, AJ, 122, 2458
 Belczynski K., Kalogera V., Rasio F. A., Taam R. E., Zezas A., Bulik T., Maccarone T. J., Ivanova N., 2005, preprint (astro-ph/0511811)
 Bell E. F., de Jong R. S., 2001, ApJ, 550, 212
 Bellazzini M., Pasquali A., Federici L., Ferraro F. R., Fusi Pecci F., 1995, ApJ, 439, 687
 Benacquista M. J., 2006, LRR, 9, 2
 Bender R., et al., 2005, ApJ, 631, 280
 Bildsten L., Deloye C. J., 2004, ApJ, 607, L119
 Binney J., Merrifield M., 1998, Galactic Astronomy, Princeton Univ. Press, Princeton, NJ
 Bregman J. N., Irwin P. S., Seitzer P., Flores M., 2006, ApJ, 640, 282
 Clark G. W., 1975, ApJ, 199, L143
 Davies M. B., Benz W., Hills J. G., 1992, ApJ, 401, 246
 de Kool M., 1990, ApJ, 358, 189
 de Marchi G., Paresce F., 1997, ApJ, 476, L19
 Deloye C. J., Bildsten L. 2003, ApJ, 598, 1217
 Devereux N. A., Price R., Wells L. A., Duric N., 1994, AJ, 108, 1667
 Dewi J. D. M., Tauris T. M., 2000, A&A, 360, 1043
 Dorman B., 1992, ApJS, 80, 701
 Dubus G., Hameury J., Charles P., 1999, MNRAS, 303, 139
 Eggleton P. P., 1983, ApJ, 268, 368
 Fabian A. C., Pringle J. E., Rees M. J., 1975, MNRAS, 172, 15
 Fregeau J. M., Cheung P., Portegies Zwart S. F., Rasio F. A., 2004, MNRAS, 358, 572
 Fryer C. L., Woosley S. E., 1999, 526, 152
 Galletti S., Federici L., Bellazzini M., Fusi Pecci F., Macrina S., 2004, A&A 416, 917
 Gilfanov M., 2004, MNRAS, 349, 146
 Girardi L., Bertelli G., Bressan A., Chiosi C., Groenewegen M. A. T., Marigo P., Salasnich B., Weiss A., 2002, A&A, 391, 195
 Grimm H-J., Gilfanov M. R., Sunyaev R. A., 2003, MNRAS, 339, 793
 Grindlay J., ASP conf. Ser. 48, The Globular Clusters-Galaxy connection, ed. G. H. Smith & J. P. Brodie (San Francisco:ASP), 156
 Grindlay, J. E., Camilo, F., Heinke, C. O., Edmonds, P. D., Cohn, H., Lugger, P. 2002, ApJ, 581, 470
 Han C., 1996, ApJ, 472, 108
 Harris W. E., 1996, AJ, 112, 1487
 Heggie D. C., 1975, MNRAS, 173, 729
 Heggie D. C., Hut, P., 1993, ApJS, 85, 347
 Hills J. G., 1976, MNRAS, 175, 1
 Hurley J. R., Tout C. A., Pols O. R., 2002, MNRAS, 329, 897

- Hut P., Bahcall J. N., 1983, *ApJ*, 268, 319
- Ivanova, N., Taam, R., 2003, *ApJ*, 599, 516
- Ivanova N., Rasio F. A., Lombardi J. C., Dooley K. L., Proulx Z. F., 2005, *ApJ*, 621, L109
- Ivanova N., Kalogera V., 2006, *ApJ*, 636, 985
- Jarret T. H., Chester T., Cutri R., Schneider S., Huchra, J. P. 2003, *AJ*, 125, 525
- Kent S.M., 1989, *AJ*, 97, 1614
- Kim E., Kim D.-W., Fabbiano G., Lee M. G., Park H. S., Geisler D., Dirsch B., 2006, *ApJ*, 647, 276
- King A. R., Frank J., Kolb U., Ritter H., 1997, *ApJ*, 484, 844
- King I. R., Sosin C., Cool A. M., 1995, *ApJ*, 452, L33
- Kochanek C. S., 1992, *ApJ*, 385, 604
- Kroupa P., 2001, *MNRAS*, 322, 231
- Kumar P., Goodman J., 1996, *ApJ*, 466, 946
- Kundu A., Maccarone T. J., Zepf S. E., 2002, *ApJ*, 574, L5
- Landau L. D., Lifshitz E. M., 1962, *The Classical Theory of Fields*, Addison-Wesley, Reading, Massachusetts
- Lee H. M., Ostriker J. P., 1986, *AJ*, 310, 176
- Liu Q. C., van Paradijs J., van den Heuvel E. P. J., 2001, *A&A*, 368, 1021
- Lombardi J. C., Proulx Z. F., Dooley K. L., Theriault E. M., Ivanova N., Rasio F. A., 2006, *ApJ*, 640, 441
- Lorimer D.R., 2005, *LRR*, 8, 7
- Lugger P.M., Cohn H.N., Grindlay J.E., 1995, *ApJ*, 439, 191
- Maccarone T. J., Kundu A., Zepf S. E., 2003, *AJ*, 586, 814
- Macri L. M., et al., 2001, *ApJ*, 549, 721
- Mardling R. M., 1995, *ApJ*, 450, 732
- McClure R. D., et al., 1986, *ApJ*, 307, L49
- McElroy D. B., 1983, *AJ*, 270, 485
- McLaughlin D.E., *ApJ*, 539, 618
- McMillan S. L. W., Taam R. E., McDermott P. N., 1990, *ApJ*, 354, 190
- Moretti A., Campana S., Lazzati D., Tagliaferri G., 2003, *ApJ*, 588, 696
- O'leary R. M., Rasio F. A., Fregeau J. M., Ivanova N., O'shaugnessy R., 2006 *ApJ*, 637, 937
- Muno M.P., Pfahl E., Baganoff F.K., Brandt W.N., Ghez A., Lu J., Morris M.R., 2005, *ApJ*, 622, L113
- Paczynski B., 1977, *ApJ*, 216, 822
- Peters P. C., 1964, *Phys. Rev.*, 136, B1224
- Pfahl E., Rappaport S., Podsiadlowski P., 2002, *ApJ*, 573, 283
- Piotto G., Zoccali M., 1999, *A&A*, 345, 485
- Piro A. L., Bildsten L., 2002, *ApJ*, 571, 103
- Podsiadlowki P., *MNRAS*, 279, 1104
- Podsiadlowki P., Rappaport S., Pfahl E. D., 2002, *ApJ*, 565, 1107
- Portegies Zwart S. F., Yungelson L. R., 1997, *A&A*, 332, 173
- Press W. H., Teukolsky S. A., 1977, *ApJ*, 213, 183
- Pryor C., Meylan G., 1993, in *ASP Conf. Ser. 50, Structure and Dynamics of Globular Clusters*, ed. S. G. Djorgovski & G. Meylan (San Francisco:ASP), 357
- Rappaport S., Verbunt F., Joss P. C., 1983, *ApJ*, 275, 713
- Rasio F. A., Shapiro S. L., 1991, *ApJ*, 377, 559
- Riffeser A., Fliri J., Seitz S., Bender R., 2005, *ApJS*, 163, 225
- Salaris M., Weiss A., 2002, *A&A*, 388, 492
- Sarazin C. L., Kundu A., Irwin J. A., Sivakoff G. R., Blanton E. L., Randall S. W., 2003, *AJ*, 595, 743
- Spitzer L., 1969, *ApJ*, 158, L139
- Spruit H. C., Ritter H., 1983, *A&A*, 124, 267
- Stanek K. Z., Garnavich P. M., 1998, *ApJ*, 503, L131
- Stehle R., Ritter H., Kolb U., 1996, *MNRAS*, 279, 581
- Taam R.E., Ricker, P.M., 2006, Preprint (astro-ph/0611043)
- van den Heuvel, E. P. J., 1992, in *Saas-Fee advanced course 22, Interacting Binaries*, ed. H. Nussbaumer & A. Orr (Springer-Verlag), 263
- Verbunt F., 1987, *ApJ*, 312, L23
- Vesperini E., Heggie D. C., 1997, *MNRAS*, 289, 898
- Voss R., Gilfanov M., 2006, *A&A*, 447, 71
- Voss R., Gilfanov M., 2007, Preprint (astro-ph/0610649)
- Voss R., Tauris T. M., 2003, *MNRAS*, 342, 1169
- Walterbos R. A. M., Kennicutt R. C., 1987, *A&AS*, 69, 311
- Webbink R. F., 1984, *ApJ*, 277, 355
- Widrow L. M., Perrett K. M., Suyu S. H., 2003, *ApJ*, 588, 311
- Yungelson L. R., Lasota J.-P., Nelemans G., et al. 2006, *A&A*, 454, 559
- Zahn J.-P., 1989, *A&A*, 220, 112
- Zahn J.-P., 1989, *A&A*, 223, 112
- Zoccali M., Cassisi S., Frogel J. A., Gould A., Ortolani S., Renzini A., Rich M. R., Stephens A. W., 2000, *AJ*, 530, 418

This paper has been typeset from a $\text{\TeX}/\text{\LaTeX}$ file prepared by the author.